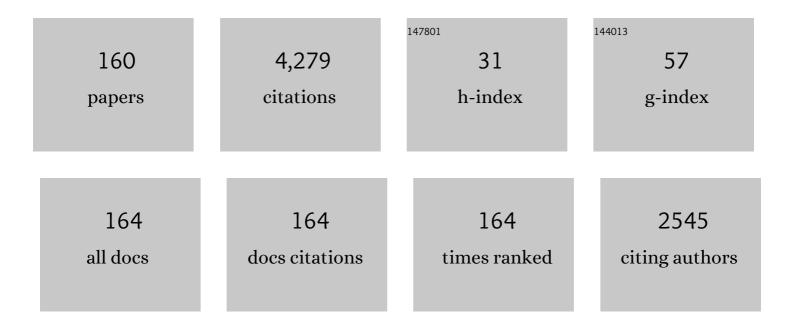
Stefan Will

List of Publications by Year in descending order

Source: https://exaly.com/author-pdf/2982052/publications.pdf Version: 2024-02-01



STEEAN W/ILL

#	Article	IF	CITATIONS
1	Laser-induced incandescence: recent trends and current questions. Applied Physics B: Lasers and Optics, 2006, 83, 333-354.	2.2	427
2	Laser-induced incandescence: Particulate diagnostics for combustion, atmospheric, and industrial applications. Progress in Energy and Combustion Science, 2015, 51, 2-48.	31.2	295
3	Modeling laser-induced incandescence of soot: a summary and comparison of LII models. Applied Physics B: Lasers and Optics, 2007, 87, 503-521.	2.2	197
4	Two-dimensional soot-particle sizing by time-resolved laser-induced incandescence. Optics Letters, 1995, 20, 2342.	3.3	161
5	Performance characteristics of soot primary particle size measurements by time-resolved laser-induced incandescence. Applied Optics, 1998, 37, 5647.	2.1	127
6	Density, Surface Tension, and Kinematic Viscosity of Hydrofluoroethers HFE-7000, HFE-7100, HFE-7200, HFE-7300, and HFE-7500. Journal of Chemical & Engineering Data, 2015, 60, 3759-3765.	1.9	127
7	Soot temperature measurements and implications for time-resolved laser-induced incandescence (TIRE-LII). Combustion and Flame, 2000, 120, 439-450.	5.2	111
8	Comprehensive two-dimensional soot diagnostics based on laser-induced incandescence (LII). Proceedings of the Combustion Institute, 1996, 26, 2277-2284.	0.3	77
9	Saturated Liquid Viscosity and Surface Tension of Alternative Refrigerants. International Journal of Thermophysics, 2000, 21, 1225-1253.	2.1	73
10	A shiftedâ€excitation Raman difference spectroscopy (SERDS) evaluation strategy for the efficient isolation of Raman spectra from extreme fluorescence interference. Journal of Raman Spectroscopy, 2016, 47, 198-209.	2.5	70
11	How Sodium Chloride Salt Inhibits the Formation of CO ₂ Gas Hydrates. Journal of Physical Chemistry B, 2016, 120, 2452-2459.	2.6	65
12	On heat conduction between laser-heated nanoparticles and a surrounding gas. Journal of Aerosol Science, 2006, 37, 1696-1716.	3.8	60
13	The effect of ethanol blending on mixture formation, combustion and soot emission studied in an optical DISI engine. Applied Energy, 2015, 156, 783-792.	10.1	60
14	2D aggregate sizing by combining laser-induced incandescence (LII) and elastic light scattering (ELS). Applied Physics B: Lasers and Optics, 2009, 96, 583-592.	2.2	58
15	Raman difference spectroscopy: a non-invasive method for identification of oral squamous cell carcinoma. Biomedical Optics Express, 2014, 5, 3252.	2.9	58
16	Wide-angle light scattering (WALS) for soot aggregate characterization. Combustion and Flame, 2010, 157, 516-522.	5.2	52
17	Techno-economic analysis of combined concentrating solar power and desalination plant configurations in Israel and Jordan. Desalination and Water Treatment, 2012, 41, 9-25.	1.0	52
18	Pumped thermal energy storage with heat pump-ORC-systems: Comparison of latent and sensible thermal storages for various fluids. Applied Energy, 2020, 280, 115940.	10.1	51

#	Article	IF	CITATIONS
19	Single-shot measurement of soot aggregate sizes by wide-angle light scattering (WALS). Applied Physics B: Lasers and Optics, 2012, 106, 171-183.	2.2	50
20	Reversible Heat Pump–Organic Rankine Cycle Systems for the Storage of Renewable Electricity. Energies, 2018, 11, 1352.	3.1	45
21	The General Phase Behavior of Mixtures of 1â€Alkylâ€3â€Methylimidazolium Bis[(trifluoromethyl)sulfonyl]amide Ionic Liquids with <i>n</i> â€Alkyl Alcohols. ChemPhysChem, 2012, 13, 1860-1867.	2.1	42
22	Carnot battery: Simulation and design of a reversible heat pump-organic Rankine cycle pilot plant. Applied Energy, 2021, 288, 116650.	10.1	42
23	Thermal Diffusivity and Sound Velocity of Toluene Over a Wide Temperature Range. International Journal of Thermophysics, 1998, 19, 403-414.	2.1	40
24	Supercritical drying of aerogel: In situ analysis of concentration profiles inside the gel and derivation of the effective binary diffusion coefficient using Raman spectroscopy. Journal of Supercritical Fluids, 2016, 108, 1-12.	3.2	39
25	Impact of morphological parameters onto simulated light scattering patterns. Journal of Quantitative Spectroscopy and Radiative Transfer, 2013, 119, 53-66.	2.3	37
26	Sizing aerosolized fractal nanoparticle aggregates through Bayesian analysis of wide-angle light scattering (WALS) data. Journal of Quantitative Spectroscopy and Radiative Transfer, 2016, 184, 27-39.	2.3	37
27	On the effect of ionic wind on structure and temperature of laminar premixed flames influenced by electric fields. Combustion and Flame, 2017, 176, 391-399.	5.2	37
28	Simultaneous Measurement of Soot Mass Concentration and Primary Particle Size in the Exhaust of a DI Diesel Engine by Time-Resolved Laser-Induced Incandescence (TIRE-LII). , 1999, , .		36
29	Diffusion Modes of an Equimolar Methane–Ethane Mixture from Dynamic Light Scattering. International Journal of Thermophysics, 2000, 21, 603-620.	2.1	36
30	Investigation of soot formation and oxidation of ethanol and butanol fuel blends in a DISI engine at different exhaust gas recirculation rates. Applied Energy, 2018, 209, 426-434.	10.1	36
31	Investigation of soot formation of spark-ignited ethanol-blended gasoline sprays with single- and multi-component base fuels. Applied Energy, 2016, 181, 278-287.	10.1	34
32	Temperature-dependent luminescence characteristics of Dy3+ doped in various crystalline hosts. Journal of Luminescence, 2018, 204, 64-74.	3.1	34
33	Design aspects of a reversible heat pump - Organic rankine cycle pilot plant for energy storage. Energy, 2020, 208, 118216.	8.8	33
34	Two-phase SLIPI for instantaneous LIF and Mie imaging of transient fuel sprays. Optics Letters, 2016, 41, 5422.	3.3	31
35	Can soot primary particle size distributions be determined using laser-induced incandescence?. Applied Physics B: Lasers and Optics, 2019, 125, 1.	2.2	30
36	Effects of process parameters and anti-scalants on scale formation in horizontal tube falling film evaporators. Desalination, 2007, 204, 448-463.	8.2	29

#	Article	IF	CITATIONS
37	High-speed combustion diagnostics in a rapid compression machine by broadband supercontinuum absorption spectroscopy. Applied Optics, 2017, 56, 4443.	2.1	29
38	Deconvolution of Raman spectra for the quantification of ternary highâ€pressure phase equilibria composed of carbon dioxide, water and organic solvent. Journal of Raman Spectroscopy, 2014, 45, 246-252.	2.5	28
39	An optimized evaluation strategy for a comprehensive morphological soot nanoparticle aggregate characterization by electron microscopy. Journal of Aerosol Science, 2020, 139, 105470.	3.8	28
40	Thermophysical Properties of Binary and Ternary Fluid Mixtures from Dynamic Light Scattering. International Journal of Thermophysics, 2001, 22, 1349-1368.	2.1	27
41	Liquidâ~'Liquid Phase Behavior of Solutions of 1-Hexyl-3-methylimidazolium Bis((trifluoromethyl)sulfonyl)amide (C ₆ mimNTf ₂) in <i>n</i> -Alkyl Alcohols. Journal of Chemical & Engineering Data, 2011, 56, 1330-1340.	1.9	27
42	Temperature and water mole fraction measurements by time-domain-based supercontinuum absorption spectroscopy in a flame. Applied Physics B: Lasers and Optics, 2015, 118, 153-158.	2.2	27
43	Thermal and mutual diffusivities of fuel-related binary liquid mixtures under pre-combustion conditions. Fuel, 2019, 242, 562-572.	6.4	27
44	Liquid–Liquid Phase Behavior of Solutions of 1-Butyl-3-methylimidazolium Bis((trifluoromethyl)sulfonyl)amide (C ₄ mimNTf ₂) in <i>n</i> Alkyl Alcohols. Journal of Chemical & Engineering Data, 2011, 56, 4829-4839.	1.9	26
45	Temperature and multi-species measurements by supercontinuum absorption spectroscopy for IC engine applications. Optics Express, 2013, 21, 13656.	3.4	26
46	Phosphor thermometry in turbulent hot gas flows applying Dy:YAG and Dy:Er:YAG particles. Measurement Science and Technology, 2015, 26, 015204.	2.6	26
47	Application of a New Soot Sensor for Exhaust Emission Control Based on Time Resolved Laser Induced Incandescence (TIRE-LII). , 2000, , .		25
48	Spatially resolved flame zone classification of a flame spray nanoparticle synthesis process by combining different optical techniques. Journal of Aerosol Science, 2014, 69, 82-97.	3.8	25
49	A mobile system for a comprehensive online-characterization of nanoparticle aggregates based on wide-angle light scattering and laser-induced incandescence. Review of Scientific Instruments, 2016, 87, 053102.	1.3	25
50	Determination of the dynamic viscosity of transparent fluids by using dynamic light scattering. Applied Optics, 1993, 32, 3813.	2.1	24
51	Liquidâ~'Liquid Phase Behavior of Solutions of 1-Octyl- and 1-Decyl-3-methylimidazolium Bis(trifluoromethylsulfonyl)imide (C8,10mimNTf2) in n-Alkyl Alcohols. Journal of Chemical & Engineering Data, 2010, 55, 2030-2038.	1.9	24
52	Liquidâ^'Liquid Phase Behavior of Solutions of 1-Dodecyl-3-methylimidazolium Bis((trifluoromethyl)sulfonyl)amide (C ₁₂ mimNTf ₂) in <i>n</i> -Alkyl Alcohols. Journal of Chemical & Engineering Data, 2010, 55, 4195-4205.	1.9	24
53	Influence of electric fields on premixed laminar flames: Visualization of perturbations and potential for suppression of thermoacoustic oscillations. Proceedings of the Combustion Institute, 2015, 35, 3521-3528.	3.9	24
54	3D mapping of droplet Sauter mean diameter in sprays. Applied Optics, 2019, 58, 3775.	1.8	24

#	Article	IF	CITATIONS
55	The release of CO2 in MSF and ME distillers and its use for the recarbonation of the distillate: a comparison. Desalination, 2005, 182, 99-110.	8.2	22
56	Generation of high-energy, kilohertz-rate narrowband tunable ultraviolet pulses using a burst-mode dye laser system. Optics Letters, 2018, 43, 1191.	3.3	22
57	Plasma-Assisted Biomass Gasification with Focus on Carbon Conversion and Reaction Kinetics Compared to Thermal Gasification. Energies, 2018, 11, 1302.	3.1	21
58	Life Cycle Assessment of a Reversible Heat Pump–Organic Rankine Cycle–Heat Storage System with Geothermal Heat Supply. Energies, 2020, 13, 3253.	3.1	21
59	4D temperature measurements using tomographic two-color pyrometry. Optics Express, 2021, 29, 5304.	3.4	21
60	Dynamic viscosity measurements by photon correlation spectroscopy. International Journal of Thermophysics, 1995, 16, 433-443.	2.1	20
61	Performance Characteristics of TIRE-LII Soot Diagnostics in Exhaust Gases of Diesel Engines. , 2000, , .		19
62	Optical diagnostics on sooting laminar diffusion flames in microgravity. Microgravity Science and Technology, 2005, 16, 333-337.	1.4	19
63	Influence of Sodium Chloride on the Formation and Dissociation Behavior of CO ₂ Gas Hydrates. Journal of Physical Chemistry B, 2017, 121, 8330-8337.	2.6	19
64	Analysis of LIF and Mie signals from single micrometric droplets for instantaneous droplet sizing in sprays. Optics Express, 2018, 26, 31750.	3.4	19
65	In-situ Measurement of Primary Particle Sizes during Carbon Black Production. Chemical Engineering and Technology, 2003, 26, 966-969.	1.5	18
66	Scale Formation and Mitigation of Mixed Salts in Horizontal Tube Falling Film Evaporators for Seawater Desalination. Heat Transfer Engineering, 2015, 36, 750-762.	1.9	18
67	Determination of Vapor–Liquid Equilibrium Data in Microfluidic Segmented Flows at Elevated Pressures Using Raman Spectroscopy. Analytical Chemistry, 2015, 87, 8165-8172.	6.5	18
68	Supercontinuum based absorption spectrometer for cycle-resolved multiparameter measurements in a rapid compression machine. Applied Optics, 2016, 55, 4564.	2.1	18
69	Investigation of mixture formation in a diesel spray by tracer-based laser-induced fluorescence using 1-methylnaphthalene. Proceedings of the Combustion Institute, 2017, 36, 4497-4504.	3.9	18
70	Viscosity of liquidn-heptane by dynamic light scattering. International Journal of Thermophysics, 1997, 18, 1339-1354.	2.1	17
71	Thermal Diffusivity and Sound Speed of the Refrigerant R143a (1,1,1-Trifluoroethane). International Journal of Thermophysics, 2001, 22, 1021-1033.	2.1	17
72	Application of Laser-Induced Incandescence for the Determination of Primary Particle Sizes of Nanoparticles Demonstrated Using Carbon Blacks. Chemical Engineering and Technology, 2002, 25, 1160-1164.	1.5	17

#	Article	IF	CITATIONS
73	Influence of EGR and ethanol blending on soot formation in a DISI engine. Proceedings of the Combustion Institute, 2019, 37, 4965-4972.	3.9	17
74	Characterization of Nile Red as a Tracer for Laser-Induced Fluorescence Spectroscopy of Gasoline and Kerosene and Their Mixture with Biofuels. Sensors, 2019, 19, 2822.	3.8	16
75	Particle diffusion in porous media investigated by dynamic light scattering. Microporous and Mesoporous Materials, 2009, 125, 63-69.	4.4	15
76	CHAPTER 2. Optical Methods. , 0, , 19-74.		15
77	Burst-mode OH/CH ₂ O planar laser-induced fluorescence imaging of the heat release zone in an unsteady flame. Optics Express, 2018, 26, 18105.	3.4	15
78	Analysis of ethanol and butanol direct-injection spark-ignition sprays using two-phase structured laser illumination planar imaging droplet sizing. International Journal of Spray and Combustion Dynamics, 2019, 11, 175682771877249.	1.0	15
79	Soot aggregate sizing in an extended premixed flame by high-resolution two-dimensional multi-angle light scattering (2D-MALS). Applied Physics B: Lasers and Optics, 2019, 125, 1.	2.2	15
80	Characterization of fuel/water mixtures and emulsions with ethanol using laser-induced fluorescence. Applied Optics, 2020, 59, 1136.	1.8	15
81	Improvement in soot concentration measurements by laser-induced incandescence (LII) through a particle size correction. Combustion and Flame, 2008, 153, 650-654.	5.2	14
82	Investigations on Soot Formation in Heptane Jet Diffusion Flames by Optical Techniques. Microgravity Science and Technology, 2010, 22, 499-505.	1.4	14
83	Systematic Investigation of the Influence of Ethanol Blending on Sooting Combustion in DISI Engines Using High-Speed Imaging and LII. , 0, , .		14
84	Phase-specific Raman spectroscopy for fast segmented microfluidic flows. Lab on A Chip, 2014, 14, 2910-2913.	6.0	14
85	Application of the tracer combination TEA/acetone for multi-parameter laser-induced fluorescence measurements in IC engines with exhaust gas recirculation. Proceedings of the Combustion Institute, 2015, 35, 3783-3791.	3.9	14
86	Multiparameter Characterization of Aerosols. Chemie-Ingenieur-Technik, 2018, 90, 923-936.	0.8	14
87	Droplet sizing in spray flame synthesis using wide-angle light scattering (WALS). Applied Physics B: Lasers and Optics, 2020, 126, 1.	2.2	14
88	Title is missing!. International Journal of Thermophysics, 1999, 20, 791-803.	2.1	13
89	Combustion and Sooting Behavior of Spark-Ignited Ethanol–Isooctane Sprays under Stratified Charge Conditions. Energy & Fuels, 2016, 30, 6080-6090.	5.1	13
90	Raman microspectroscopy and multivariate data analysis: optical differentiation of aqueous d- and l-tryptophan solutions. Physical Chemistry Chemical Physics, 2017, 19, 30533-30539.	2.8	13

#	Article	IF	CITATIONS
91	Impact of Oxygenated Additives on Soot Properties during Diesel Combustion. Energies, 2021, 14, 147.	3.1	13
92	Spectroscopic determination of selected thermophysical properties of transparent fluids. Measurement: Journal of the International Measurement Confederation, 1994, 14, 135-145.	5.0	12
93	Thermophysical Properties of Fluids from Dynamic Light Scattering. International Journal of Thermophysics, 2001, 22, 317-338.	2.1	12
94	Synthesis and Characterization. Lecture Notes in Physics, 2009, , 1-82.	0.7	12
95	One-dimensional Raman spectroscopy and shadowgraphy for the analysis of the evaporation behavior of acetone/water drops. International Journal of Heat and Mass Transfer, 2015, 89, 406-413.	4.8	12
96	(Gd,Lu)AlO ₃ :Dy ³⁺ and (Gd,Lu) ₃ Al ₅ O ₁₂ :Dy ³⁺ as high-temperature thermographic phosphors. Measurement Science and Technology, 2019, 30, 034001.	2.6	12
97	Inferring soot morphology through multi-angle light scattering using an artificial neural network. Journal of Quantitative Spectroscopy and Radiative Transfer, 2020, 251, 106957.	2.3	12
98	Three-dimensional particle size determination in a laminar diffusion flame by tomographic laser-induced incandescence. Applied Physics B: Lasers and Optics, 2021, 127, .	2.2	12
99	Light scattering by surface waves on a vertical layer of liquid toluene. Applied Optics, 1997, 36, 7615.	2.1	11
100	Determination of several thermophysical properties of toluene using a single experimental setup. Fluid Phase Equilibria, 1999, 161, 337-351.	2.5	11
101	ESA's Drop Tower Utilisation Activities 2000 to 2011. Microgravity Science and Technology, 2011, 23, 409-425.	1.4	11
102	Simultaneous two-dimensional measurement of fuel–air ratio and temperature in a direct-injection spark-ignition engine using a new tracer-pair laser-induced fluorescence technique. International Journal of Engine Research, 2016, 17, 120-128.	2.3	11
103	Analysis of the LIF/Mie Ratio from Individual Droplets for Planar Droplet Sizing: Application to Gasoline Fuels and Their Mixtures with Ethanol. Applied Sciences (Switzerland), 2019, 9, 4900.	2.5	11
104	Dynamic light scattering system with a novel scattering cell for the measurement of particle diffusion coefficients. Review of Scientific Instruments, 1996, 67, 3164-3169.	1.3	10
105	Thermophysical properties of R143a (1,1,1-trifluoroethane). International Journal of Refrigeration, 2001, 24, 734-743.	3.4	10
106	A Raman technique applicable for the analysis of the working principle of promoters and inhibitors of gas hydrate formation. Journal of Raman Spectroscopy, 2015, 46, 1145-1149.	2.5	10
107	Novel electric thermophoretic sampling device with highly repeatable characteristics. Review of Scientific Instruments, 2016, 87, 125108.	1.3	10
108	Fluorescence characteristics of the fuel tracers triethylamine and trimethylamine for the investigation of fuel distribution in internal combustion engines. Applied Optics, 2016, 55, 1551.	2.1	10

#	Article	IF	CITATIONS
109	Characterization of a silica-aerosol in a sintering process by wide-angle light scattering and principal component analysis. Journal of Aerosol Science, 2018, 119, 62-76.	3.8	10
110	Planar droplet sizing for studying the influence of ethanol admixture on the spray structure of gasoline sprays. Experiments in Fluids, 2020, 61, 1.	2.4	10
111	Characterization of the phosphor (Sr,Ca)SiAlN3: Eu2+ for temperature sensing. Journal of Luminescence, 2020, 226, 117487.	3.1	10
112	Simulation of the Part Load Behavior of Combined Heat Pump-Organic Rankine Cycle Systems. Energies, 2021, 14, 3870.	3.1	10
113	Characterization of YAG:Dy,Er for thermographic particle image velocimetry in a calibration cell. Measurement Science and Technology, 2017, 28, 025013.	2.6	9
114	In situ analysis of aerosols by Raman spectroscopy – Crystalline particle polymorphism and gas-phase temperature. Journal of Aerosol Science, 2018, 126, 143-151.	3.8	9
115	The Effect of Ethanol Blending on Combustion and Soot Formation in an Optical DISI Engine Using High-speed Imaging. Energy Procedia, 2015, 66, 77-80.	1.8	8
116	Thermo-fluid dynamic model for horizontal packed bed thermal energy storages. Energy Procedia, 2017, 135, 51-61.	1.8	8
117	In Situ Determination of Droplet and Nanoparticle Size Distributions in Spray Flame Synthesis by Wide-Angle Light Scattering (WALS). Materials, 2021, 14, 6698.	2.9	8
118	Luminescence Properties of the Thermographic Phosphors Dy ³⁺ :YAG and Tm ³⁺ :YAG for the Application in High Temperature Systems. Zeitschrift Fur Physikalische Chemie, 2015, 229, 977-997.	2.8	7
119	Investigation of Soot Formation in a Novel Diesel Fuel Burner. Energies, 2019, 12, 1993.	3.1	7
120	UV absorption cross sections of vaporized 1-methylnaphthalene at elevated temperatures. Applied Physics B: Lasers and Optics, 2020, 126, 1.	2.2	7
121	Characterisation of the transition type in optical band gap analysis of in-flame soot. Combustion and Flame, 2022, 243, 111986.	5.2	7
122	Atom optics with Bose–Einstein condensates: quantum reflection and interferometry. Journal of Physics: Conference Series, 2005, 19, 139-145.	0.4	6
123	Influence of ethanol admixture on the determination of equivalence ratios in DISI engines by laser-induced fluorescence. Applied Optics, 2016, 55, 8532.	2.1	6
124	Investigations on particle diffusion in porous glass by angle-dependent dynamic light scattering. Journal of Molecular Liquids, 2016, 222, 972-980.	4.9	6
125	Stability Analysis of the Fluorescent Tracer 1-Methylnaphthalene for IC Engine Applications by Supercontinuum Laser Absorption Spectroscopy. Sensors, 2020, 20, 2871.	3.8	6
126	Laserinduzierte Inkandeszenz (LII) zur Partikelgrößenbestimmung von aggregierten Rußpartikeln. Chemie-Ingenieur-Technik, 2009, 81, 803-809.	0.8	5

#	Article	IF	CITATIONS
127	Supercontinuum high-speed cavity-enhanced absorption spectroscopy for sensitive multispecies detection. Optics Letters, 2016, 41, 2322.	3.3	5
128	Temperature determination of superheated water vapor by rotational-vibrational Raman spectroscopy. Optics Letters, 2018, 43, 4477.	3.3	5
129	Application of FRAME for Simultaneous LIF and LII Imaging in Sooting Flames Using a Single Camera. Sensors, 2020, 20, 5534.	3.8	5
130	Measurement of Water Mole Fraction from Acoustically Levitated Pure Water and Protein Water Solution Droplets via Tunable Diode Laser Absorption Spectroscopy (TDLAS) at 1.37 µm. Applied Sciences (Switzerland), 2021, 11, 5036.	2.5	5
131	Measurement of Secondary Structure Changes in Poly-L-lysine and Lysozyme during Acoustically Levitated Single Droplet Drying Experiments by In Situ Raman Spectroscopy. Sensors, 2022, 22, 1111.	3.8	5
132	CO2 release in vertical tube falling film evaporators. Desalination, 2008, 222, 626-638.	8.2	4
133	Potential of two-line atomic fluorescence for temperature imaging in turbulent indium-oxide-producing flames. Journal of Nanoparticle Research, 2015, 17, 1.	1.9	4
134	Fluorescence characteristics of the fuel tracer 1-methylnaphthalene for the investigation of equivalence ratio and temperature in an oxygen-containing environment. Applied Physics B: Lasers and Optics, 2019, 125, 1.	2.2	4
135	Shifted-excitation rotational Raman spectroscopy and Bayesian inference for in situ temperature and composition determination in laminar flames. Journal of Quantitative Spectroscopy and Radiative Transfer, 2020, 249, 106996.	2.3	4
136	In situ characterisation of absorbing species in stationary premixed flat flames using UV–Vis absorption spectroscopy. Applied Physics B: Lasers and Optics, 2021, 127, 1.	2.2	4
137	Broadband Two-Color Laser-Induced Incandescence Pyrometry Approach for Nanoparticle Characterization with Improved Sensitivity. Applied Spectroscopy, 2013, 67, 1098-1100.	2.2	3
138	Raman excess spectroscopy vs. principal component analysis: probing the intermolecular interactions between chiral molecules and imidazolium-based ionic liquids. Physical Chemistry Chemical Physics, 2016, 18, 28370-28375.	2.8	3
139	Investigating the Moisture Content of Polyamide 6 by Raman-Microscopy and Multivariate Data Analysis. Physics Procedia, 2016, 83, 1271-1278.	1.2	3
140	Correlation of the kinetics of aggregation and inactivation of L-glutamate dehyrogenase during drying and particle formation of a levitated microdroplet. Drying Technology, 2019, 37, 164-172.	3.1	3
141	Spatially-resolved crystallinity determination of polymer welding seams by Raman-microscopy. Procedia CIRP, 2020, 94, 796-801.	1.9	3
142	3D mapping of polycyclic aromatic hydrocarbons, hydroxyl radicals, and soot volume fraction in sooting flames using FRAME technique. Applied Physics B: Lasers and Optics, 2021, 127, 1.	2.2	3
143	Measurement of particle diffusion coefficients with high accuracy by dynamic light scattering. Progress in Colloid and Polymer Science, 1997, 104, 110-112.	0.5	2
144	Burst-mode 1-methylnaphthalene laser-induced fluorescence: extended calibration and measurement of temperature and fuel partial density in a rapid compression machine. Applied Physics B: Lasers and Optics, 2022, 128, .	2.2	2

#	Article	IF	CITATIONS
145	Design and validation of a multimodal low-budget Raman microscope for liquid and solid phase applications. Proceedings of SPIE, 2015, , .	0.8	1
146	High-speed, inline measurement of protein activity and inactivation processes by supercontinuum attenuation spectroscopy. Analyst, The, 2019, 144, 7041-7048.	3.5	1
147	Rotational Raman spectroscopy for in situ temperature and composition determination in reactive flows. , 2019, , .		1
148	Herriott cell enhanced SMF-coupled multi-scalar combustion diagnostics in a rapid compression expansion machine by supercontinuum laser absorption spectroscopy. Optics Express, 2021, 29, 42184.	3.4	1
149	A versatile fibre-based setup for two-line atomic fluorescence thermometry in aerosol processes. Journal of Quantitative Spectroscopy and Radiative Transfer, 2022, 278, 108042.	2.3	1
150	Korngrößenanalyse in der Prozeßmeßtechnik über die Photosedimentation. Chemie-Ingenieur-Technik, 1995, 67, 113-117.	0.8	0
151	Measurement of particle diffusion coefficients with high accuracy by dynamic light scattering. , 1997, , 110-112.		0
152	Die dynamische Lichtstreuung als universelle Meßtechnik zur Bestimmung von Stoffdaten am Beispiel von Toluol. Chemie-Ingenieur-Technik, 1999, 71, 257-261.	0.8	0
153	Start-up and operation of an integrated 10 MW/sub p/ thin film PV module factory. , 0, , .		0
154	Lichtstreuung zur Online-Charakterisierung von Nanopartikeln. Chemie-Ingenieur-Technik, 2010, 82, 1408-1409.	0.8	0
155	Flame Temperature Measurements by Time-domain Based Supercontinuum Absorption Spectroscopy. Energy Procedia, 2015, 66, 129-132.	1.8	0
156	Untersuchungen zum Einfluss von Ethanolzumischung auf die Rußbildung bei der Benzindirekteinspritzung. Proceedings, 2017, , 425-438.	0.3	0
157	Laser-induced incandescence. Applied Physics B: Lasers and Optics, 2020, 126, 1.	2.2	0
158	Commonly Asked Questions in Thermodynamics. , 0, , .		0
159	In situ monitoring of aerosols by Raman spectroscopy $\hat{a} \in ``$ particle polymorphism and gas-phase temperature. , 2018, , .		0
160	Untersuchung der Rußbildung und Rußoxidation von Ethanol- und Butanolgemischen in einem Transparentmotor mit Benzindirekteinspritzung. Proceedings, 2019, , 79-93.	0.3	0